RESEARCH ARTICLE

The evolving volcano-ice interactions of Crater Glacier, Mount St. Helens, Washington (USA)

Linda Sobolewski[1] · Thor H. Hansteen[2] · Edgar U. Zorn[3] · Christian Stenner[4] · Lee J. Florea[5] · Sarah A. Burgess[6] · Artur Ionescu[7,8,9] · Eduardo Cartaya[10] · Andreas Pflitsch[1]

Abstract

Interactions between volcanoes and glaciers provide insight to the evolution of a volcanic edifice and may be an indicator for renewed volcanic activity. At Mount St. Helens, Crater Glacier, which has formed in the volcanic crater after the eruption in 1980, is one of the world's last expanding glaciers and provides a unique opportunity to characterize the evolution of a glacier expanding onto an area of significant thermal flux. We combine photographic documentation and glaciovolcanic cave surveys with remote sensing data from Google Earth, UAS, and LiDAR to analyze the present state of Crater Glacier and reconstruct its development since the emplacement of the 2004–2008 lava dome. Our results show that snow accumulation has caused Crater Glacier to grow from 2009 to 2019 by approximately 13.8×10^6 m^3, during which time the glacier toe advanced by several hundred meters. The glacier-dome interface shift toward higher elevations against the 2004–2008 lava dome and subsequent encroachment onto thermally active areas led to glacier modification via extensive subglacial cave system formation. Analysis of subglacial tephra layers revealed the existence of juvenile material from the 2004–2008 eruption cycle, providing insights about glacier subsidence of ~40 m since 2004/2005 in spite of net growth. Although the lava dome is cooling, the glacier-dome interface seems to have become increasingly stable in the past few years. Our results suggest that glacier development in the accumulation area adjacent to the dome is now being affected by the thermal characteristics of the lava dome itself, making monitoring internal glacier development via tracking glaciovolcanic cave expansion a potentially important volcano monitoring tool.

Keywords Glaciovolcanism · Debris-covered glaciers · Glacier-lava dome interplay · Subglacial tephra layers

Zusammenfassung

Die Interaktionen von Vulkanen und Gletschern tragen häufig zum Verständnis über die Entwicklung eines vulkanischen Systems bei und können als Indikator für wiederkehrende vulkanische Aktivität dienen. Crater Glacier, der nach der Eruption 1980 im Krater des Mount St. Helens entstanden ist, ist einer der letzten wachsenden Gletscher weltweit und bietet somit eine einmalige Chance, die Entwicklung eines Gletschers in Verbindung mit erheblichen Wärmeflüssen zu charakterisieren. Neben einer fotografischen Dokumentation des Gletschers machen wir uns die Kartierung vulkanischer Gletscherhöhlen zu

---

✉ Linda Sobolewski
  linda.sobolewski@ruhr-uni-bochum.de

1 Ruhr University Bochum, Bochum, Germany

2 GEOMAR Helmholtz Centre for Ocean Research Kiel, Kiel, Germany

3 German Research Centre for Geosciences GFZ, Potsdam, Germany

4 Alberta Speleological Society, Calgary, AB, Canada

5 Department of Natural Resources, Washington State Geological Survey, Olympia, WA, USA

6 Bloomington Indiana Grotto, National Speleological Society, Bloomington, IN, USA

7 Faculty of Biology and Geology, Department of Geology, Babes-Bolyai University, Cluj-Napoca, Romania

8 Department of Physics and Geology, University of Perugia, Perugia, Italy

9 Institute for Nuclear Research, International Radiocarbon AMS Competence and Training Center (INTERACT), Debrecen, Hungary

10 Glacier Cave Explorers, National Speleological Society, Redmond, OR, USA

Nutze. Diese kombinieren wir mit Fernerkundungsdaten von Google Earth sowie Drohnen- und LiDAR-Daten, um den aktuellen Zustand des Gletschers zu charakterisieren und seine Entwicklung seit dem letzten Lavadomwachstum zwischen 2004 und 2008 zu rekonstruieren. Unsere Ergebnisse zeigen, dass die ausreichende Akkumulation von Schnee zum Wachstum des Gletschers mit einem Massenzuwachs von ca. 13,8 x 10^6 m^3 zwischen 2009 und 2019 geführt hat. Neben dem Voranschreiten der Gletscherzunge um mehrere hundert Meter hat sich das Wachstum ebenfalls rund um den neuen Lavadom bemerkbar gemacht. Durch die Verschiebung der Kontaktzone von Gletscher und Lavadom hin zu höheren Bereichen des Doms und der damit verbundenen Interaktion zwischen Gletscher und geothermaler Aktivität ist es zu einer deutlichen Veränderung des Gletschers durch die Ausbildung subglazialer Höhlensysteme gekommen. Analysen von im Gletscher eingebetteten Tephraschichten, die vermutlich der letzten Aktivität zwischen 2004 und 2008 zuzuordnen sind, deuten trotz des allgemeinen Wachstums auf eine Setzung des Gletschers um etwa 40 m seit 2004/05 hin. Obwohl der Lavadom an Hitze verliert, scheint die Kontaktzone von Gletscher und Dom in den letzten Jahren zunehmend konstant geworden zu sein. Unsere Ergebnisse deuten darauf hin, dass der Gletscher in diesem Bereich derzeit vor allem durch die thermalen Eigenschaften des Lavadoms beeinflusst wird. Dadurch kommt dem Monitoring interner Gletscherstrukturen mittels Beobachtung vulkanischer Gletscherhöhlen eine potenziell wichtige Bedeutung bei der Vulkanüberwachung zu.

Introduction

Following the cataclysmic eruption of Mount St. Helens on May 18, 1980, and the formation of a north-facing, horseshoe-shaped crater and lava dome growth between 1980 and 1986, a new glacier formed in the crater protected from sunlight by steep headwalls and partly insulated by a debris cover (Schilling et al. 2004; Walder et al. 2008). This advancing glacier is called "Crater Glacier" (Walder et al. 2008). Between 2004 and 2008, renewed volcanic activity and the emplacement of a new lava dome changed the glacier, bisecting and compressing it against the crater walls. As a result, glacier surface speed increased and the east arm of the glacier nearly doubled in thickness (Price and Walder 2007).

Before the 2004–2008 Mount St. Helens activity, lava dome emplacement through a glacier was poorly understood. A single photo from the caldera glacier recorded dome emplacement at Great Sitkin Volcano (Alaska) in 1945 (Walder et al. 2008). In contrast, volcano-ice interactions at Mount St. Helens were closely studied following the 1980 crater formation, including through the 2004–2008 eruption period. For example, Schilling et al. (2004) described the post-1980 glacier development, using

aerial photos and digital elevation models (DEMs) to calculate snow accumulation rates and glacial volume. Price and Walder (2007) and Walder et al. (2007; 2008; 2010) then described the effects of lava dome growth on the glacier from 2004–2008. Studies include the investigation of morphological changes of the glacier and lava dome using DEMs, the analysis of glacier surface motion through a flowband model and photography. Additional DEMs which include pre-eruption data from 2000 and data collected between 2004 and 2007 were provided by Messerich et al. (2008). The subsequent formation of rock glaciers on the east flank of Crater Glacier and the transformation of the glacier toe into a rock or debris-covered glacier were discussed by Schilling et al. (2004), Gutro and Puckett (2004), and Gabrielli et al. (2020).

Void spaces in firn and ice (glaciovolcanic caves) can form concurrently with advancing glaciers on lava domes as a result of thermal flux. Anderson et al. (1998) and Anderson and Vining (1999) first described this phenomenon at Mount St. Helens and investigated a system of melt passages in firn encircling the 1980–1986 lava dome. These passages were destroyed by the 2004–2008 activity, and another system of glaciovolcanic caves has formed in the past decade. These caves are still evolving and encircle the 2004–2008 lava dome (Sobolewski et al. 2022).

Investigations of glacier development and of volcano-ice interactions following the 2004–2008 lava dome emplacement are largely lacking. For instance, it is unclear what modifications to the glacier are occurring, especially due to recent glacier encroachment against the lava dome. Similarly, subglacial hydrogeology remains unstudied except as an intersection between aqueous geochemistry and volcanic heat flux in a variety of thermal springs adjacent to the glacier terminus and on the pumice plain (Bergfeld et al. 2008). Furthermore, the interplay between volcanism and meteorology on the glacier and within glaciovolcanic caves is not well understood, which may become considerably relevant as increasingly frequent heat waves occur in the U.S. Pacific Northwest. Fieldwork within the crater to make on-site observations is challenging due to the hazardous environment. Rockfall originating from the crater walls and rim constantly lands on the glacier surface, while crevasses and typical glacier hazards are compounded when investigating subglacial voids. The same rockfall debris reappears and melts out of cave walls and ceilings, while collapse of cave ceilings is another risk.

Here, we describe the post 2008 development of the Mount St. Helens crater and glacier by combining on-site observations from 2014 to 2021 and resulting surveys from physical exploration of subglacial cave systems as well as remote sensing imagery, aerial LiDAR data, and UAS-based (UAS = Unoccupied Aircraft System) photogrammetry. In addition, we analyze the chemical compositions of subglacial tephra layers observed in one of the glaciovolcanic caves to reconstruct the motion and surface

subsidence of Crater Glacier and to identify juvenile dome compositions. The idea is to use the tephra layers as an approximate but novel indicator for glacier subsidence/melt and to combine volcanological and glaciological aspects to further characterize volcano-ice interactions. The studies presented here provide insight into the dynamics of an advancing glacier in times of global glacier retreat. From a volcanological perspective, glaciovolcanic interactions reveal insights into the current state of the volcanic edifice and are valuable volcano monitoring tools.

Methods and datasets

On-site observations and time series remote sensing data using Google Earth images

On-site quantification of the cave systems and enclosing glacier started in 2014, including inter-annual assessments of subglacial cave scale and morphology and a multi-year survey of the glacier surface. These observations include aerial and surface photography of the environment in the crater. Images in this paper were taken from 2014 to 2021 and focus on the area south of the 2004–2008 lava dome where the glacier and lava dome directly interact (accumulation area). Attention is also given to structures observed on the glacier surface and the features of the glacier toe (ablation area).

Optical-range satellite remote sensing data accessible via Google Earth at regular time intervals dating back several decades was of varying quality and resolution. We exploited regular image availability (2004–2021) to track and evaluate glacier changes over time. This allowed direct measurements of ice cover and position (via the ruler tool), including the advancing glacier toe and the advance of the rock-ice interface around the new lava dome. Image analysis also allowed identification of supraglacial ponds and glacier surface structures. Moreover, the imagery was helpful to identify conspicuous surface features on ice-free areas of the new lava dome. Although Google Earth is becoming increasingly important in earth sciences and it has already been used for volcano monitoring (Bailey and Dehn 2006), Google Earth does not make any statements or guarantees about the accuracy. Thus, the results presented in this article are estimates and do not reveal precise/georeferenced data/measurements. From 2012 to 2021, however, Google Earth images have a good quality with a high resolution which increases the accuracy of measurements. A table with image dates and original data sources is included (Supplementary Table S1).

Evaluation of digital elevation data from LiDAR and UAS photogrammetry

LiDAR data sets for the Mount St. Helens crater from 2004 to 2007, 2009, 2017, and 2019 were freely available from the Washington LiDAR Portal (Department of Natural Resources 2022) and the U.S. Geological Survey data release (Mosbrucker 2014; 2020). Data sets from 2009, 2017, and 2019 were processed in QGIS and ArcGIS to create DEMs and calculate changes in glacier volume. Resolutions were indicated as 9.45 points/m^2 for the 2009 data and 4.79 points/m^2 for the 2019 data with root mean square errors (RSME) of 0.035 m and 0.061 m, respectively. No formal accuracy assessments were conducted for the 2017 data set. LiDAR data were also used to investigate the uppermost part of the glacier south of the new lava dome (accumulation area). Using DEMs for the glacier surface following the 2004–2008 lava dome emplacement, this information was used to calculate approximately glacier surface subsidence since that time. The subsidence was estimated using tephra layers embedded in the glacier as temporal marker horizons.

We further constrained an orthophoto map at a local scale using a DJI Mavic Air 2S UAS in June 2021 to acquire 824 aerial images (all in nadir) over the southern glacier-dome interface. Using structure-from-motion photogrammetry (Westoby et al. 2012; James et al. 2020a) in Agisoft Metashape (version 1.8.0), we built an orthophoto with a 1.15-cm ground resolution. This gave a more detailed view of the surface and structures compared to the satellite image resolution and could be further used to assess surface flow directions. This was indicated by the thin tephra/debris accumulation covering the snow and the orientation of that accumulated material visible on the glacier surface. Although the alignment of the accumulated debris results from surface melting processes, comparative imagery of it can be used as an indicator for the overall glacier movement in this specific part of the volcanic crater.

While the spatial resolution is very high, the geolocation of the model is less accurate as we could only use a single ground control point taken with a handheld GNSS device (Garmin InReach Explorer +); hence, the model location is expected to be accurate to within 5–10 m. This and the nadir only acquisition also leave the model vulnerable to further distortion errors such as surface doming (James et al. 2020b); however, as our map only covers a small portion of the dome and glacier (< 500 m), these are likely negligible. As we do not use the orthomap for quantitative measurements and only visually assess surface flow patterns, we do not expect that there are errors to impact our results.

Geospatial quantification of cave systems

The above methods were combined with data on subglacial voids at the glacier-dome interface. Glaciovolcanic cave systems were surveyed 2014–2021 to understand the extent and shape of subglacial cavities to identify areas where heat

from the 2004–2008 lava dome interacts with the advancing glacier. Survey methods are described by Sobolewski et al. (2022) and Stenner et al. (2022) and included tacheometric measurements using DistoX2 captured in Topodroid software and processed in Compass cave survey software. Cave entrances were georeferenced via handheld GNSS. The data from these cave surveys allowed subglacial void spaces to be located and characterized in three dimensions, including cave depths and lengths and estimation of the volume of void space in the ice. Survey methods used allow error ratios of 0.05 m for survey shot length, 1° for azimuth and inclinometer measurements, and 2% overall, while accuracy of entrance positions is within 3 m. Combined with an inventory of features in the caves, such as fumarolic areas, subglacial waterfalls, or ice tunnels, a detailed picture of the subglacial landscape was possible.

Cave tephra sampling and electron microprobe analysis

Subglacial retrieval of tephra was possible by accessing it from within Mothra Cave in June 2021. The samples were extracted with a hammer and a chisel from a cave wall located deep inside the cave. Geopositioned sample locations and depths in the glacier were obtained and cross referenced with cave survey data. To avoid contamination of tephra with eroded, superficial material on the cave walls, relevant surface areas were cleaned prior to sampling. We extracted four samples (A–D). Samples A, B, and C derive from different horizontal layers sub-parallel to the cave floor. Sample D was taken from a lens of tephra in direct proximity to the horizontal layers.

Due to the challenging sampling conditions, the amount of extracted particles for each sample was limited. A statistically valid grain size distribution analysis was thus rendered questionable, and a visual grain size distribution assessment using each bulk sample was preferred. Furthermore, each of the samples was shown to be dominated by particles not originating from the present Mount St. Helens dome, further questioning the value of accurate grain size distribution data on such polygenetic and re-deposited samples.

The glassy groundmass in sampled tephra particles was analyzed for major and minor elements on epoxy-embedded mounts using a JEOL JXA 8200 wavelength dispersive electron microprobe (GEOMAR, Kiel). A calibrated acquisition program was used based on international standards (Jarosewich et al. 1980). We used an acceleration voltage of 15 kV, a beam current of 6 nA, and a slightly defocused beam of 5 μm diameter. Peak counting times were 20 s for all elements except Na. To minimize Na loss, Na was measured first, with peak counting times of 5 s. Oxide concentrations were determined using the ZAF correction method.

Accuracy was monitored by two measurements each on Lipari obsidian (Lipari rhyolite; Hunt and Hill 2001) and Smithsonian basaltic standard VGA99 (Makaopuhi Lava Lake, Hawaii; Jarosewich et al. 1980) following every 30–40 point measurements. Standard deviations are $< 0.5\%$ for major and $< 10\%$ for minor elements, with the exception of P_2O_5 and MnO_2 in samples > 65 wt% SiO_2. All analyses with totals > 95 wt% were normalized to 100% in order to eliminate the effects of minor deviations in focusing of the electron beam and possible post-depositional hydration (Supplementary Table S2). The accepted analyses of each sample were then averaged in order to characterize the elemental compositions of each tephra particle.

Compositional (element) maps for Al were acquired for selected tephra particles. The pixel size used was 3 μm, and counting time 500 μs per pixel, using the WDS detector mode.

Results

Visual characterization and on-site observations

Crater Glacier is still growing and subject to significant rock fall from the surrounding crater walls (Fig. 1a, c). Photographs from 2019 illustrate the extent of the glacier in the crater (Fig. 1a), the position of the glacier toe (Fig. 1b), and the presence of rock glaciers at scree slopes at the east side of the crater wall (Fig. 1a). Smaller rock glaciers also exist at the west side of the crater wall. Crevasses and bergschrund-like features are present on both the east and the west glacier arms (Fig. 1a). Lower elevation parts of the glacier (north of the 1980–1986 lava dome to the glacier toe) include considerable debris cover, in some parts more than one meter thick (Fig. 1d). Clear differences between the accumulation and ablation areas of the glacier exist. While the accumulation area has a thin and patchy debris cover, the coverage significantly increases toward lower elevations in the north and is visible at the glacier arms (Fig. 1a).

We observed increasing interactions between the snow/firn and fumaroles after 2014 along with glacier advance toward the 2004–2008 lava dome and subsequent interactions with higher elevations of the dome. One typical feature includes glacier depressions at the contact zone between the glacier and the lava dome (Fig. 1e). Another is crevasse-like fractures on the glacier surface and the formation of openings as observed in 2014 (Fig. 1f). Crater Glacier exhibits very dynamic inter-annual variations, demonstrated by significantly changing surface structures and the modification of cave entrance morphology. But, although morphology of surface structures may change rapidly, their existence (with differing inter-annual morphology) can persist for years.

Using UAS images and a high-resolution orthophoto, we visualized the surface flow of Crater Glacier in the accumulation area south of the 2004–2008 lava dome (Fig. 2). Surface structures suggest limited movement toward both the east and the west glacier arms. Rather, surface flow primarily orients toward the lava dome or the crater wall, according to the elevation profile. Cave entrances on the orthophoto partially show crevasse-like features on the glacier surface or an abrupt and sharp edge of the rock-ice interface indicated by shading of these areas.

We experienced a record heat wave in the Pacific Northwest during 2021 fieldwork. This resulted in temperatures 3 °C greater than the previous Seattle record of 39 °C and 6 °C above previous records further inland with extremes of 49 °C in June 2021 (Overland 2021). We recorded maximum air temperatures of 18 °C 30 cm above the glacier ice. A clearly observable response by the glacier was indicated by strong surface ablation during a short timeframe of June 22–28. A small firn field located between the two lava domes to the east showed a surface loss of ~ 25 cm per day.

Analyses of Google Earth images

Images archived on Google Earth illustrated the advance of the glacier toe and were used to calculate the increase in glacier area (Fig. 3a). From June 2006 to June 2009, the glacier gained approximately 0.23 km^2 in surface area. Both the west and the east arms of the glacier merged, forming only one glacier toe that is thickened at its end. In some areas, the glacier advanced more than 500 m in 3 years. This trend continued between June 2009 and August 2012. In the years following through 2021, glacier growth progressed, but at a significantly lower rate. Google Earth image comparison revealed movement of the rock-ice interface on the new lava dome (Fig. 3b). The most noticeable shift is 2009–2011, followed by the period from 2011 to 2018. Only minor changes were present from 2018 to 2021. However, all images indicate glacier growth and expansion on the lava dome ranging from a few tens of meters up to more than one hundred meters. One isolated spot south of the lava dome (entrance area of Rodan/Hedorah/Ghidorah caves) appears to have a near-constant rock-ice margin, and no obvious shift is visible between 2009 and 2021 (Fig. 3b).

We further tracked surface structures of Crater Glacier over time and investigated their persistence. Two time series were generated—one showing the entrance area of Rodan/Hedorah/Ghidorah caves and the location of Godzilla Hole and the other one showing an entrance to Crevasse Cave (Fig. 4). The 2004 image (first time series) illustrates the situation at the start of the 2004–2008 eruption cycle. Near Rodan/Hedorah/Ghidorah caves, noticeable structures on the glacier surface have been arising since 2006, initially indicated by fracturing of the glacier. Through 2021, a steep edge had formed and grown. At Godzilla Hole, a similar steep edge evolved from 2006 to 2011 followed by the formation of a cave entrance 2012–2014 (opening of the glacier
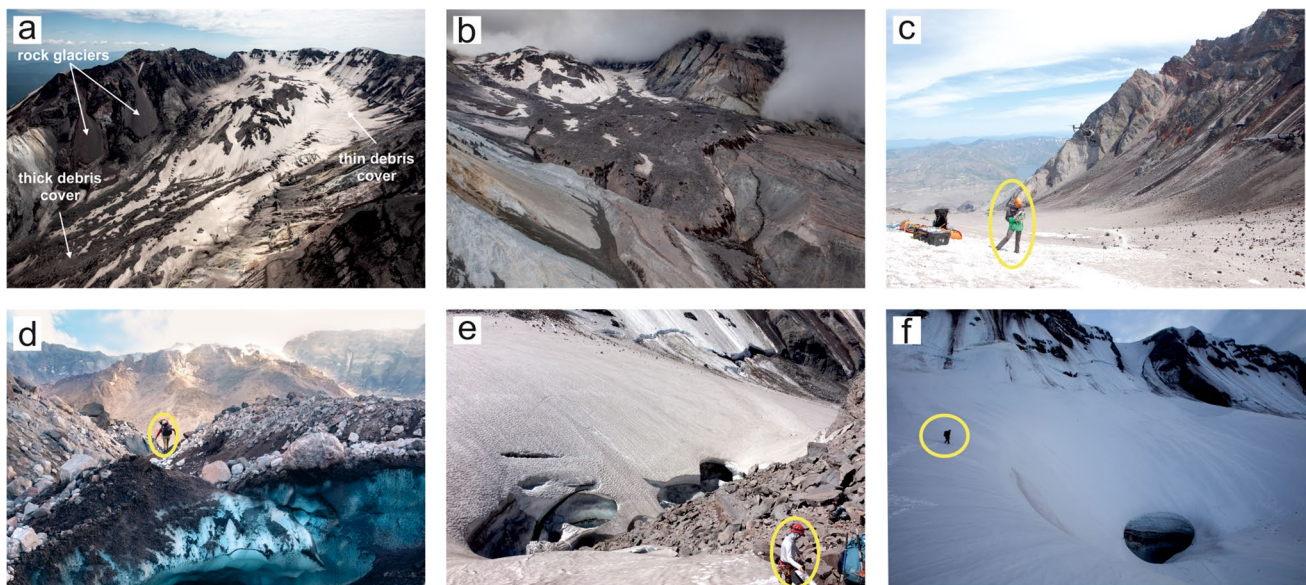

Fig. 1 Photographic documentation of Crater Glacier from May 2014 to June 2021. **a** Aerial photo of the Mount St. Helens' Crater showing the two lava domes in the center of the crater, the surrounding glacier, and rock glaciers, June 2018. **b** Aerial photo of Crater Glacier and its thickened, debris-covered glacier toe, June 2019. Photos: Eric Guth (used with permission). **c** Rockfall on the east glacier arm, June 2018. Photo: Linda Sobolewski. **d** Thick debris cover north of the 1980–1986 lava dome, August 2019. Photo: Jared Smith (used with permission). **e** Entrance area of Rodan/Hedorah/Ghidorah caves, June 2021. Photo: Linda Sobolewski. **f** Chimney entrance of Godzilla Hole (partial collapse of the cave ceiling), June 2014. Photo: Brent McGregor (used with permission)
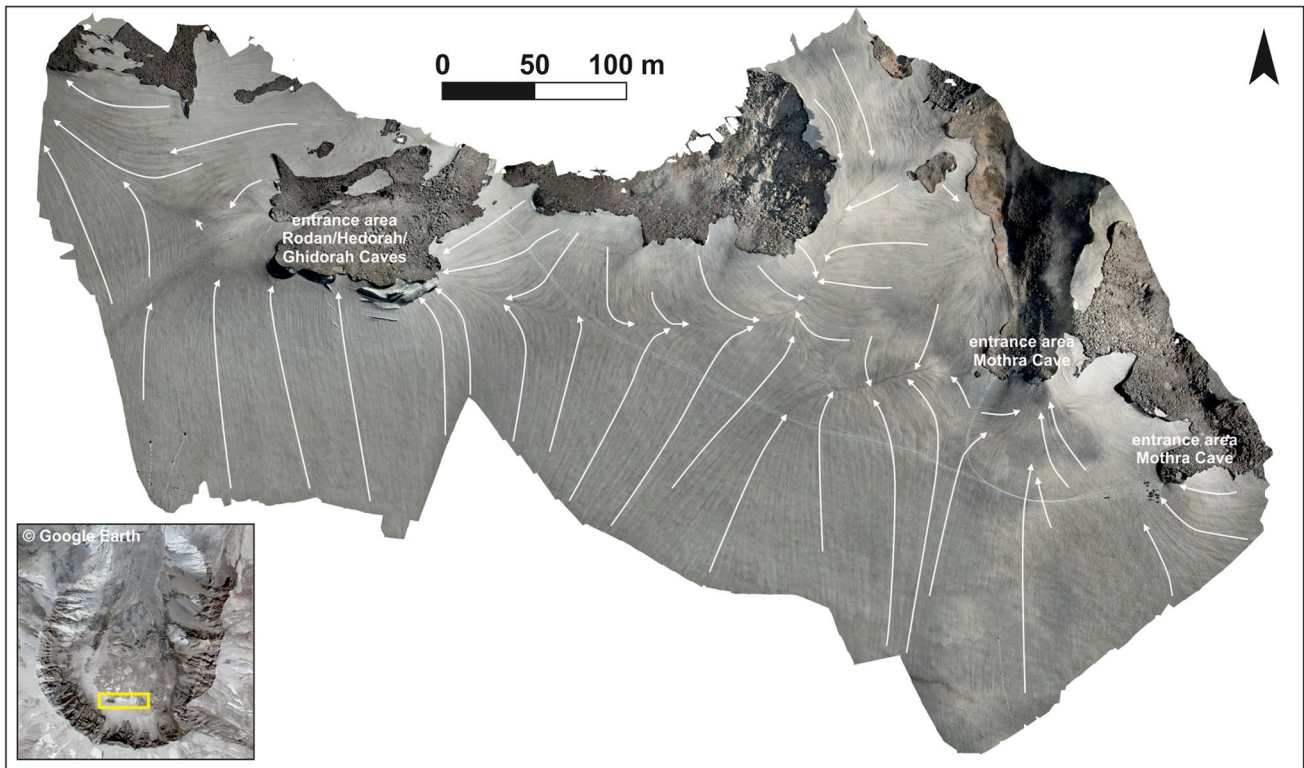
Fig. 2 High-resolution orthophoto generated from drone images. The photo shows the area south of the 2004–2008 lava dome with the entrance area of Rodan/Hedorah/Ghidorah caves. White arrows indi-cate the surface flow direction of Crater Glacier as seen on the ortho-photo. Drone images were taken in June 2021 by Jason Nelson and were used with permission

surface) as the glacier advanced toward the upper parts of the lava dome. More recently, this opening was filled, chang-ing into a depression 2016–2017 and finally disappeared in 2021. Similar observations were made at one of the entrance areas of Crevasse Cave 2012–2021. While only the rock sur-face was visible in 2012, a small cavity evolved in the fol-lowing years and is visible in images from 2014 to 2017. This cavity was supplemented by significant crevasses, vis-ible in 2018 and 2021. The glacier advance from 2012 to 2021 is also visible.

In addition to observations of the glacier surface, Google Earth also allowed the identification of distinct structures arising on the new lava dome (Fig. 5). The lava dome surface either shows a darker color (wet ground) persistent for years (Fig. 5a) or a mixture of wet ground, steam emanations, and discoloration of the ground (Figs. 5b, c). Steam ema-nations were visible in 2017 (Fig. 5b) and 2016 (Fig. 5c). An example of greenish or reddish-brownish coloring of the ground is visible in 2014 (Fig. 5b) and 2016 (Fig. 5c), indicating hydrothermal alteration or algae. Images available on Google Earth from 2012 to 2021 represent the spring/summer season as they were taken between May and August. Thus, they do not show the appearance of the lava dome with an extensive snow cover. However, even annual changes of

the remaining snow during the spring and summer season most likely indicate that specific dome areas permanently remain snow-free.

Supraglacial ponds have formed on the debris cover in the ablation area north of the 1980–1986 lava dome toward the glacier toe (Supplementary Figure S3). These ponds are present during the summer melt months and can have dimen-sions of up to ~36 m as seen on a recent image from July 2021. Google Earth images indicate a start of supraglacial pond formation in 2009 with the number and extent con-stantly increasing.

Mapping of subglacial cave systems

By 2021, more than 3 km (3009 m) of mapped cave passage encircled the perimeter of the new lava dome (Fig. 6) with a total volume of 1.57×10^5 $m^3 \pm 2\%$. Since the start of repeat cave surveys in 2014, the caves have revealed a dynamic morphology and expanded significantly, most visible when viewing comparative surveys from 2014 and 2021. The bulk of subglacial void spaces is located south of the 2004–2008 lava dome; however, some caves were also mapped west of the new dome (Cloaca) and in the northeastern section between the 2004–2008 and the 1980–1986 domes (Igloo,

Gigan, Dogora). One cave was mapped east of the new lava dome and is heavily affected by glacier movement with crevasse-like features on the glacier surface (Crevasse, Lower Crevasse). Structures are clearly visible on aerial images and in the field. Cave survey results and comparison between different years also indicate the influence of glacier movement. Previous studies of the Mount St. Helens caves and further cave descriptions are presented by Sobolewski et al. (2022).

Melting glacier ice focused more intensely around fumarolic activity, and therefore, the glaciovolcanic caves continuously recharge the thick package of subglacial sediment. This groundwater interacts with and flushes volcanic heat and dissolved gases toward the thermal springs at lower elevation. Unlike mapped glaciovolcanic caves at Mount Hood that, prior to melt out, supported an active subglacial conduit and englacial stream (Pflitsch, unpublished data), no englacial streams persist in the glaciovolcanic caves of Mount St. Helens. As such, they are significant recharge points for subglacial groundwater, but do not significantly influence groundwater flow.

Mothra Cave, the second longest cave in the crater, is located south of the 2004–2008 lava dome and was surveyed in 2018, 2019, and 2021, with a length and depth of 594 m and 65 m, respectively, as of 2021 (Fig. 7). Cave passages were observed to be highly dynamic with obvious morphology changes from 2018 to 2021. Cave passages significantly expanded toward the south (Fig. 8) with fumarolic activity being present in the newly formed passages (Fig. 7). Although fumaroles were also observed from 2018 to 2019 (in the deepest cave part), a clear shift of fumarole locations was observed in 2021, concurrent with cave expansion to the south. For detailed comparison between the different years, see also Sobolewski et al. (2022). In 2021, Mothra Cave had a total volume of 38×10^3 m$^3 \pm 2\%$. Characteristic features, as observed in previous years, include multiple tephra layers embedded in the glacier, ice tunnels, and subglacial waterfalls.

Comparison of digital elevation models

LiDAR data clearly show that Crater Glacier has gained volume, with a significant accumulation area located south of the new lava dome (Fig. 9). From 2009 to 2017, glacier volume increased by nearly 11.4×10^6 m^3. From 2017 to 2019, another ~2.4×10^6 m^3 were added. Glacial advance is also visible at the glacier toe, while glacier ablation was observed at the glacier arms. Both the glacial toe and margins are strongly influenced by crevasses. LiDAR data were also used to further investigate the uppermost part of the glacier (area of Mothra Cave), which resulted in two key observations: (1) Mothra Cave could not have started forming prior to 2009 considering the position of ice on the lava dome (i.e., there was no ice before 2009), and (2) elevation profiles indicate that after a major disruption of the glacier in 2004/2005, the glacier surface finally regained the smooth and regular pre-eruption shape but with significant elevation increase. Profiles in 2000 and 2017 have nearly the same shape and show a parallel offset (Fig. 8). Similar observations regarding the position of the ice-lava dome interface and the start of cave formation apply to all other caves except for Igloo, Gigan, and Dogora. Evidence is provided by LiDAR data and Google Earth images combined with cave mapping results. While observation (1) is already discussed in the study by Sobolewski et al. (2022), LiDAR results in this work provide more detailed insight. Furthermore, combining observation (2) with the determination of a temporal (subglacial) marker horizon via compositional studies of tephra particles in discrete layers allows us to estimate a net surface glacier subsidence of ~40 m since 2004/2005.

Descriptions of subglacial tephra layers

Each of the investigated subglacial tephra layers contains a variety of particles covering a range of morphologic features, crystallinity, and textures and is therefore interpreted as a polygenetic volcaniclastic layer. The tephra layers further reveal a spectrum of grain sizes. Samples from layers A and B are dominated by comparatively small grain sizes (ca. 10–200 µm). Maximum sizes of the less frequent large particles in layer A are up to 1 mm and up to 500 µm in layer B, respectively. The sample from layer C is characterized by the absence of fine particles, and the typical grain sizes range from 200 µm to more than 1 mm. Layer D shows the poorest sorting and includes a spectrum of particle sizes between ca. 10 µm and a few millimeters. While samples from A, B, and C showed a regular layering with specific grain sizes being dominant in each layer, the sample from D was characterized by a mixture of various fragments without showing any dominating grain sizes. Layers A, B, and C show a good sorting within each layer and horizontal accumulation sub-parallel to the cave floor. Layer D represents a lens of tephra particles without any discernible sorting or regular deposition (Fig. 10). Geopositioned sample locations (Fig. 7) record the layer depths at −50 m from the cave entrance.

All samples comprise particles with blocky, vesicular, and elongated morphologies, covering particles with a crystallized groundmass, phenocryst-rich ones with variably glassy groundmass, and glass-dominated, pumiceous particles (Supplementary Table S2). This study focuses on particles with a glassy groundmass, in order to use a combination of textures, mineral contents, and glass compositions to address the provenance of volcanic particles. Such particles range from glass-dominated to phenocryst-dominated, the latter ones with variable amounts of groundmass microlites
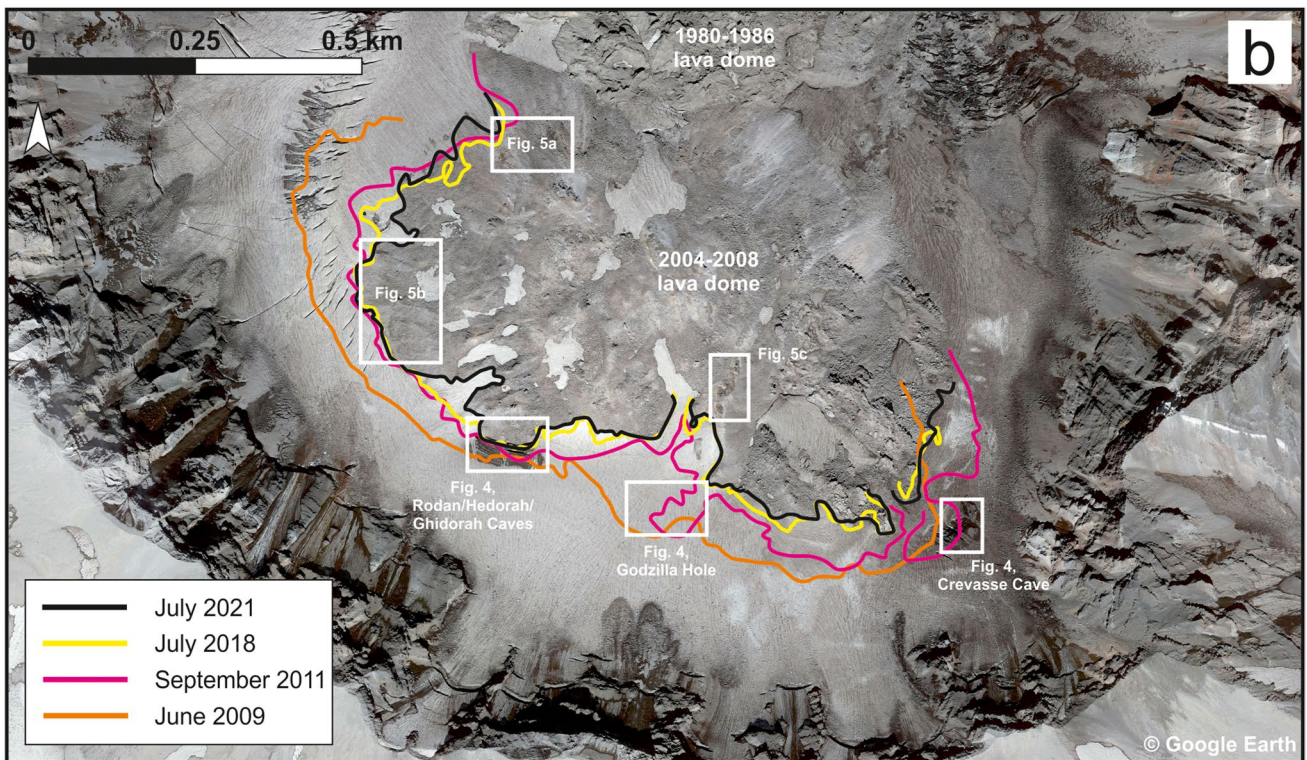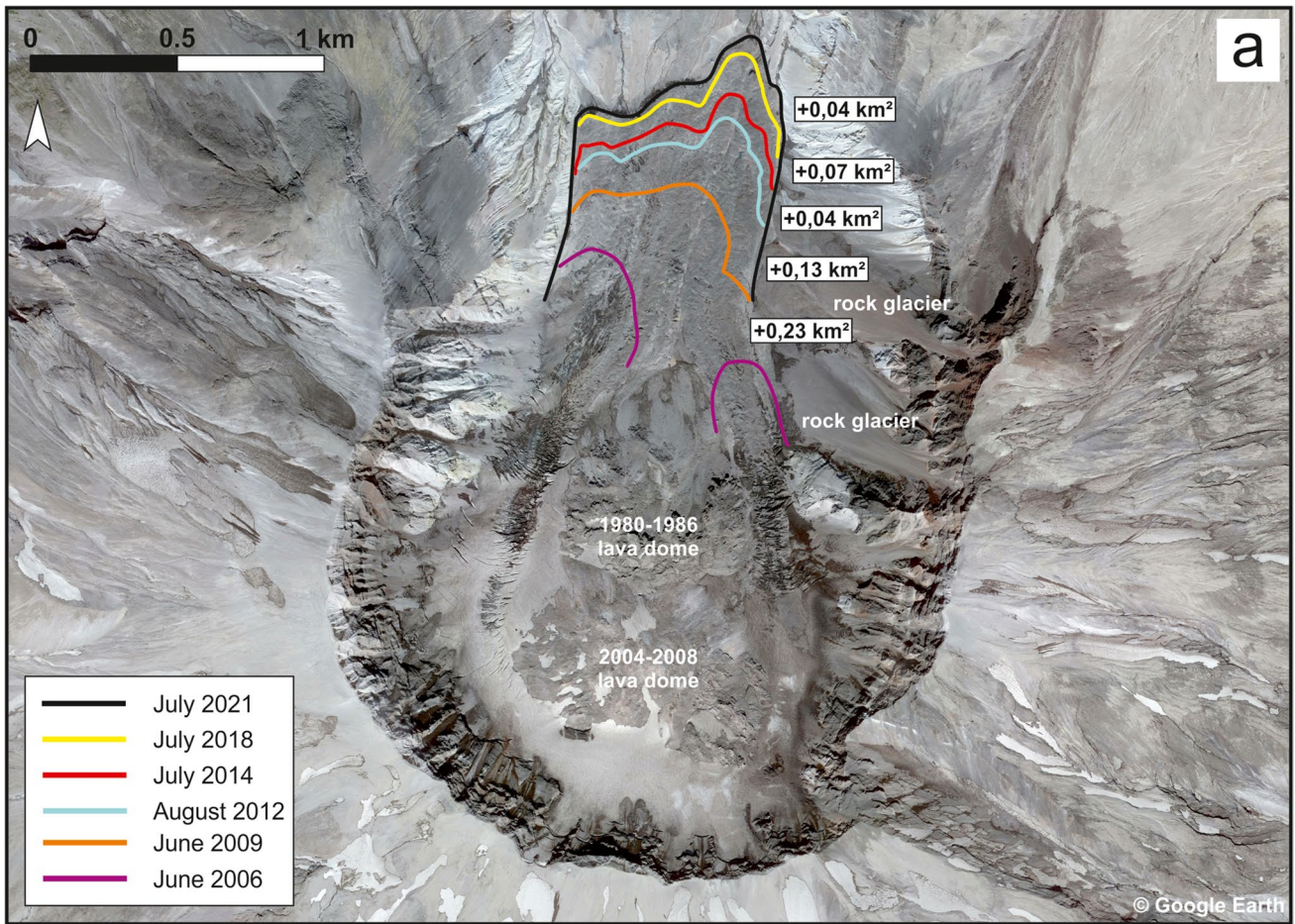
◄**Fig. 3** Advance of Crater Glacier as seen on Google Earth imagery. **a** Advance of the glacier toe from June 2006 to July 2021. Numbers in white boxes indicate the increase in area between different years. **b** Advance toward the 2004–2008 lava dome from June 2009 to July 2021. © Google Earth. White boxes indicate the location of images shown in Figs. 4 and 5

(Supplementary Figure S4). As the tephras at St. Helens have been thoroughly investigated in previous studies and detailed sample descriptions are beyond the scope of this paper, the reader is referred to Rowe et al. (2008a; b), Pallister et al. (2008), and Cashman et al. (2008) for further information.

Composition of matrix glasses in tephra particles

Typical particles with a glassy groundmass were selected from each layer for electron microprobe analysis. Analyses of "clean glass" within single grains show a broad compositional range, with two major types of glass: type 1 glasses have SiO_2 contents between 61 and 79 wt%, but predominantly contain more than 70% SiO_2, corresponding to dacites and rhyolites (Fig. 10). MgO contents are less than 1 wt%. Type 2 glasses are characterized by SiO_2 contents ranging between 52 and 61 wt% and MgO between 1.8 and 5.5 wt%, respectively (Supplementary Table S2 and Supplementary Figure S5). Following the classification of Rowe et al. (2008a) for Mount St. Helens glasses, type 1 glasses were divided into three subgroups (Fig. 10). Type 1a comprises glasses with K_2O wt% contents between 1.9 and 3.5 wt% and represents the most frequent type. Type 1b glasses have K_2O contents higher than 3.5 wt% and MgO contents of maximum 0.3 wt%. This group corresponds to the composition of Mount St. Helens´ juvenile dome glasses from the 2004–2008 activity period (Rowe et al. 2008a). We additionally recognized a third group, type 1c, which also has K_2O contents higher than 3.5 wt%, but comparatively lower SiO_2 contents than type 1b (< 70 wt%). Notably, the particles containing type 1b and 1c glasses show comparatively high glass contents and a dominance of plagioclase microlites, and thus texturally closely resemble "early erupted material" (Cashman et al. 2008), which most probably erupted in 2004.

Discussion

Crater Glacier: a debris covered glacier

Present characteristics of Crater Glacier that match typical features of debris-covered glaciers are rugged surface topographies resulting from a largely continuous layer of supraglacial debris, most notably in the ablation area and with increasing thickness toward the toe. Furthermore, these glaciers typically develop supraglacial-englacial hydrologic systems of channels and ponds (Miles et al. 2020). Although we did not specifically investigate the glacier´s englacial hydrology separate from the glaciovolcanic cave systems, we can confirm the existence of supraglacial ponds on top of the debris cover which exists north of the old lava dome and downslope to the glacier toe. According to Miles et al. (2020), it can be characterized as a "thick" layer due to a debris accumulation > 1 m (Fig. 1d). The spatial distribution and varying thickness of the debris cover on Mount St. Helens with the general trend of increasing thickness with decreasing elevation is characteristic of debris-covered glaciers as discussed by Miles et al. (2020). While snow and ice avalanches reach the upper part of the glacier, rock avalanches and significant rockfall deposits reach the mid and lower glacier areas. The changing morphology and decline in ice surface velocity toward the glacier toe represent another essential factor responsible for varying thicknesses (Anderson and Anderson 2018; Mihalcea et al. 2008).

The impact of heavy rockfall from the crater walls was considered to be a major factor for glacier formation and growth due to insulation of the underlying ice as described by Mills (1992), Schilling et al. (2004), and Walder et al. (2008). As discussed by Walder et al. (2008), however, the uppermost part of the glacier was estimated to contain no more than 5% debris by volume. Rockfall and resulting debris cover probably enhanced the onset of glacier formation in the first few years, but cannot be considered a major factor in the accumulation area for the last ~ two decades. A photo from October 2000 presented by Schilling et al. (2004) clearly indicates that a significant and continuous debris cover is not present in the areas south of the old 1980–1886 lava dome. In 2000, a thick cover is visible at both glacier arms due to substantial rock deposits from the crater walls, sufficient enough to reduce melting. We observed a similar situation during our recent field campaigns. The uppermost part of the glacier, although impacted by rockfalls (Fig. 1c), shows a thin and patchy debris cover with increasing thickness toward lower elevated areas (Fig. 1b) and the greatest accumulation at the glacier toe (Fig. 1d). We can conclude that the debris cover typical of this accumulation area is beneath the critical thickness (typically ~ 5 cm), which would inhibit superficial melting. Studies by Østrem (1959) and Nicholson and Benn (2006) treated the influence of a debris cover on glaciers and found that a cover beneath the critical thickness has an inverse effect and accelerates superficial melting in comparison to clean ice. Lundstrom et al. (1993) who investigated Eliot Glacier of nearby Mount Hood concluded that even a debris thickness as little as 2 cm can reduce the ablation rate. For Mount St. Helens, we can clearly say that such a cover (min. 2 cm) mostly now exists in the higher elevation areas. We rather suggest the opposite situation where the very thin debris cover in this area
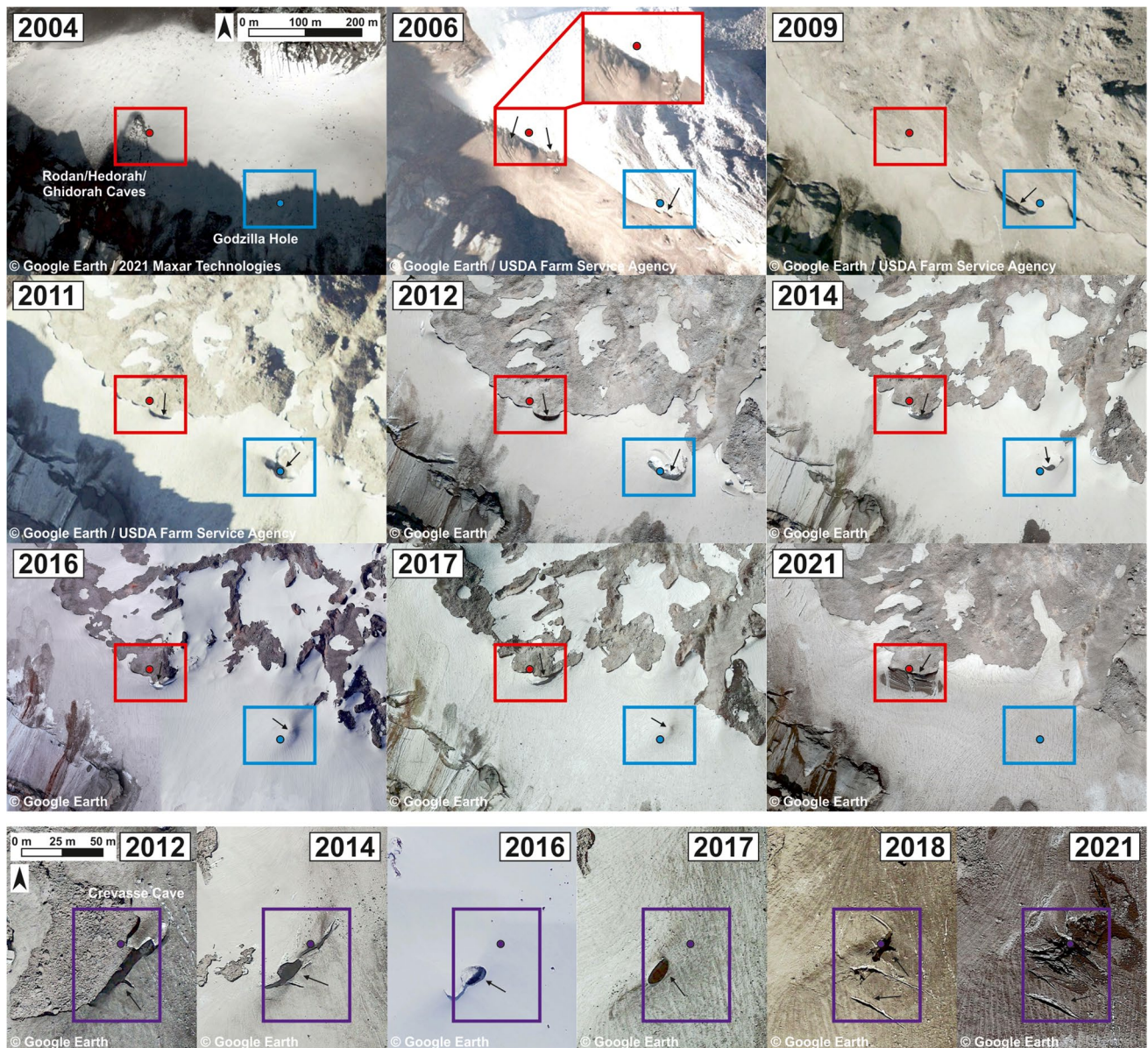
Fig. 4 Tracking of glacier surface structures using Google Earth images. Red boxes indicate the entrance location of Rodan/Hedorah/ Ghidorah caves; blue boxes the location of Godzilla Hole; purple boxes the location of Crevasse Cave. Dots in the boxes are reference points and indicate the same location on every image. © Google Earth / 2021 Maxar Technologies / USDA Farm Service Agency

advances surface melt during the ablation season. Changing climate may exacerbate ablation in these areas as observed in the extreme surface melt at the camp site area and around the new lava dome in June 2021.

As described by Østrem (1959), ablation rates under thicker debris progressively decline. This situation is expressed in the mid and lower elevation areas of Crater Glacier. Extensive debris cover is clearly visible and facilitates the formation of supraglacial ponds (Supplementary Figure S3). The supraglacial ponds are no larger than tens of meters, and thus, these are not very likely to pose a threat to the surrounding area at their current sizes. Assessments

of glacial outburst floods hazards show that glacial lakes smaller than 0.1 km^2 can usually be considered as non-hazardous (Liu et al. 2020). From the perspective of the glaciovolcanic caves, they are not conduits for water; they are sources of groundwater recharge percolating into thick subglacial debris.

Glacier expansion and volcano-ice interactions

Following the 2004–2008 eruption cycle, Crater Glacier continued to grow—the glacier toe advanced (Fig. 3a) and the glacier margin continued to advance upwards against the lava
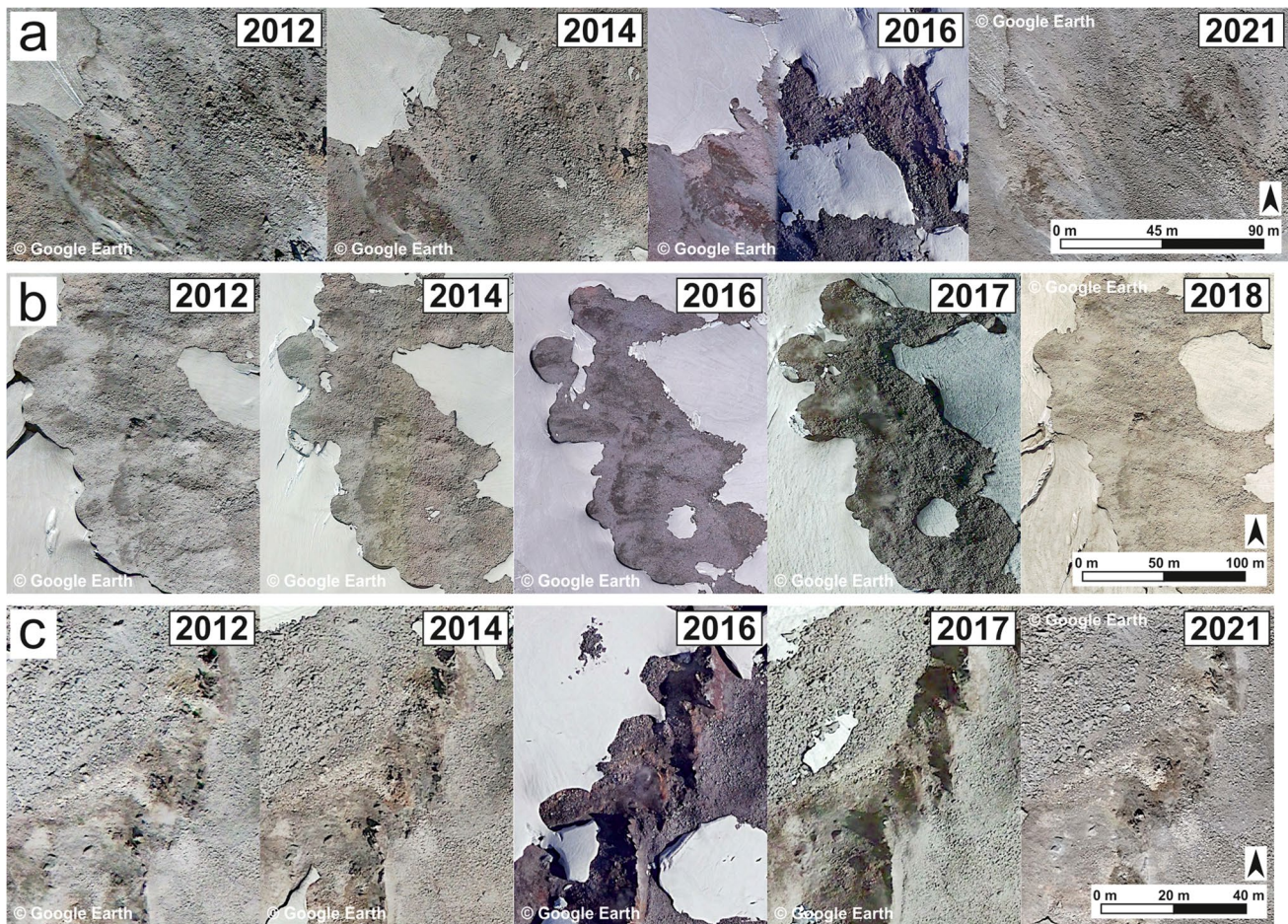
Fig. 5 Tracking of surface structures on the 2004–2008 lava dome using Google Earth images. **a** Two conspicuous areas of wet ground are existent on every image from 2012 to 2021. **b** Several areas showing wet ground (2012, 2014, 2016, 2018), steam emanations (2017), or discoloration of soil (2014). **c** Elevated areas showing wet ground are existent on every image from 2012 to 2021; steam emanations are present in 2016. © Google Earth

dome (Fig. 3b). Glacier elevation changes calculated from LiDAR data (Fig. 9) confirm that Crater Glacier continues to grow overall. An inverse process is happening internally in the glacier, however. Due to the limited movement of the glacier in the accumulation area toward the sides and a constant progress toward the new lava dome (Fig. 2), glaciovolcanic caves started to form within the last decade (Sobolewski et al. 2022). Glacial encroachment against the dome, advancing toward increasingly higher elevations, is syngenetic with the formation of extensive glaciovolcanic caves (Fig. 6) resulting from the thermal flux between the lava dome and overlying glacier. Minor changes in the rock-ice interface were observed from 2018 to 2021, suggesting a slowdown in dome-adjacent glacier expansion and perhaps reaching a steady state for these volcano-ice interactions (Fig. 3b). Although there is sufficient snow supply (Fig. 9), thermal energy from the lava dome currently is preventing further advance. Provided fumarolic output continues at similar rates and in these locations, it is unlikely that the rock-ice interface will change significantly

in the next few years. Our results indicate that focused heat release on the exposed dome itself has remained near-constant over several years, e.g., the entrance area of Rodan/Hedorah/Ghidorah caves, parts of Crevasse Cave (Fig. 4), and areas indicated in Fig. 5. The lava dome, however, appears to be cooling based on decreasing fumarole temperatures (Sobolewski et al. 2022). For instance, gradually cooling fumarole temperatures would gradually shift the balance between ice accumulation and melting, resulting in a cave size reduction over time. On the other hand, increased thermal emissions or increasing fumarole temperatures could further expand the caves, thus indirectly indicating renewed activity from the volcano.

Although our results obtained from orthophotos and the position of tephra layers within the glacier suggest a limited movement of the glacier toward the sides and a significant motion toward the new lava dome, the area of mass accumulation south of the lava dome is somewhat analogous to an ice dome which should have an ice divide separating
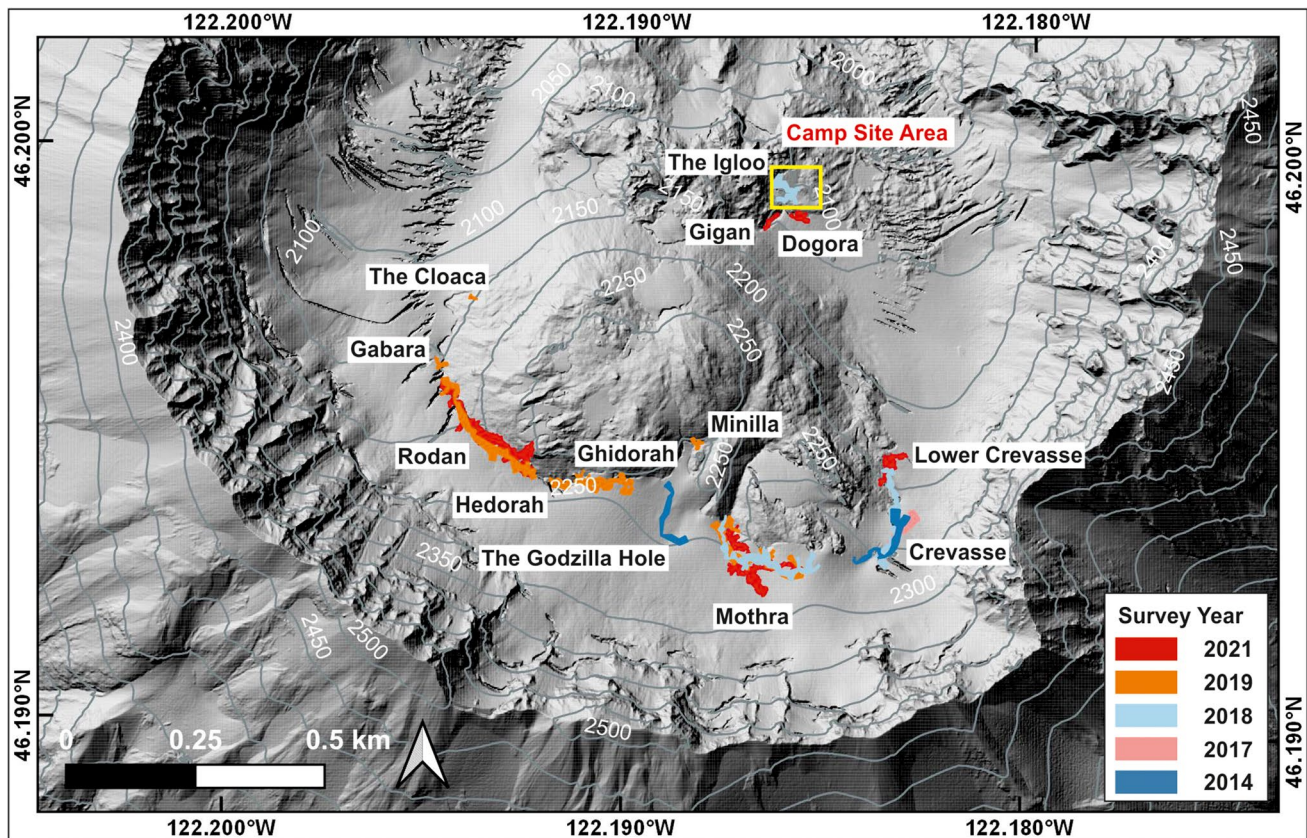
Fig. 6 Map of the Mount St. Helens crater and location of glaciovolcanic cave systems surveyed between 2014 and 2021. Total system length: 3009 m. Map was generated from LiDAR data provided by the Washington Lidar Portal and represents a digital elevation model from 2019. The yellow box indicates the camp site area

flow into the two arms of the glacier (J. Walder, personal communication). This ice divide cannot be identified on the glacier surface, but it must exist as the glacier is advancing, fed by the accumulation area south of the new lava dome. The peculiar nature of this area which is primarily fed by avalanching from the crater wall plays a significant role for glacier movement (J. Walder, personal communication).

Given the characteristics of the caves with subglacial waterfalls and continuous melt processes due to interaction with heat from the lava dome, the caves may substantially influence the hydrology of the volcano by contributing novel and constant cross seasonal meltwater input. Although the total cave system volume ($\sim 1.57 \times 10^5$ m^3) is comparatively small relative to the total glacier volume, the boundary area of the new lava dome influenced by cave systems and internal melting processes is notable. We can only speculate about the impact of meltwater on the volcano's hydrology and this needs to be confirmed by further studies. Monitoring glacier surface structures and subglacial changes within glaciovolcanic cave systems may thus become an additional tool to analyze the state of the lava dome and observe its future development. The use of optical satellite images to detect volcanic impacts on glacier surface

morphology was recently assessed by Martin et al. (2021) who highlighted the importance of improving our understanding of volcano-ice interactions. While these studies primarily focused on image assessment during an eruption, our investigations concentrate on the implications for post-eruption periods.

Spatial distribution of thermal energy release from the new dome

Combining field observations, locational data of the cave systems, and the use of Google Earth images, we were able to identify areas on the 2004–2008 lava dome that have a distinct thermal energy release. Specific examples are presented in Fig. 5. Distinct energy release here is considered to be enough heat to keep parts of the lava dome continuously snow free or maintain specific sub- and supraglacial structures for years. From visual observations alone, we were able to obtain the following information: (1) Heat release from the lava dome is not only limited to the uppermost part of the dome complex. We were able to identify numerous fumarolic areas located at the glacier-dome contact zone and lower elevation sites of the dome. (2) Heat release in some
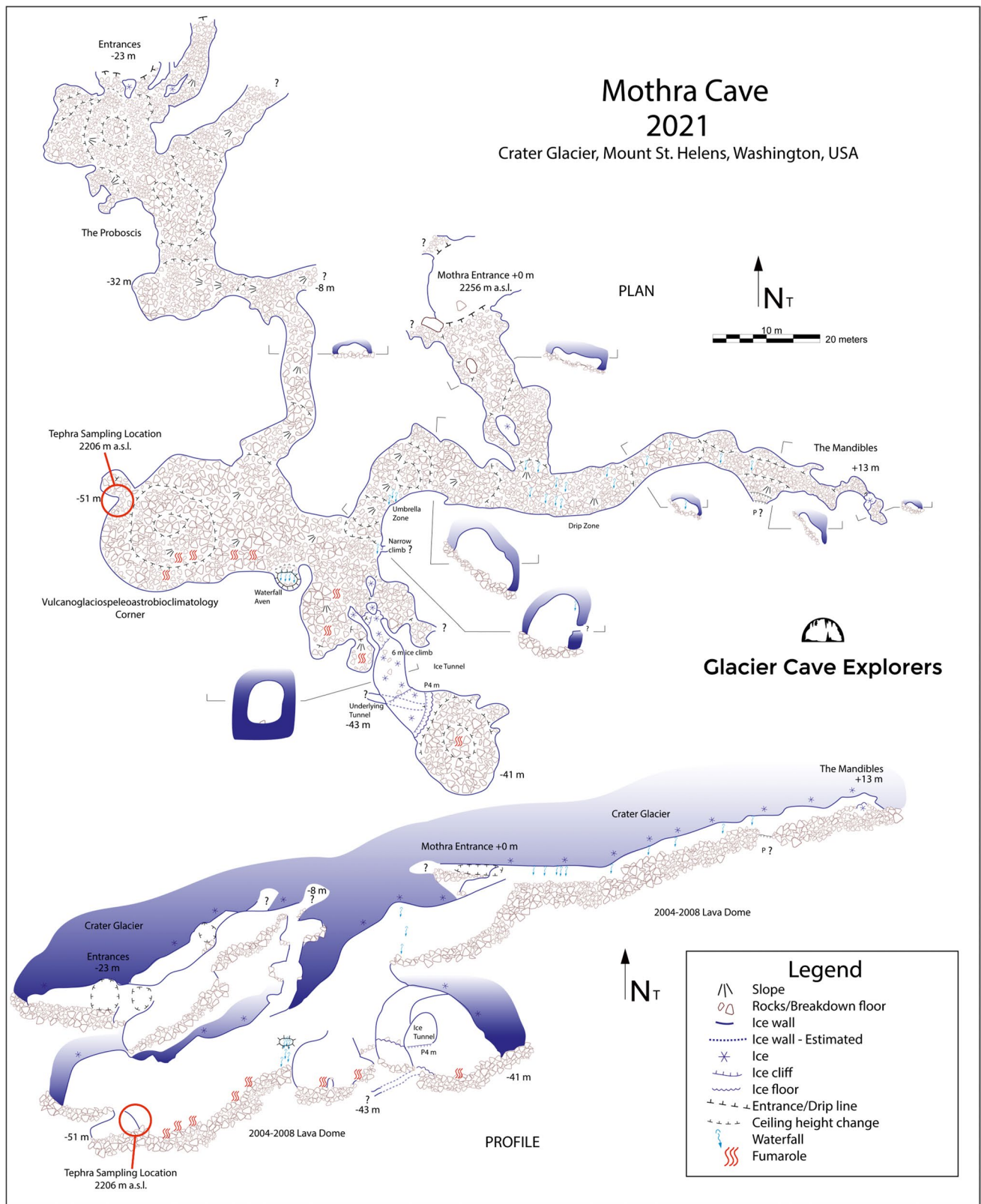
Fig. 7 Map of Mothra Cave as surveyed in June 2021 with illustration of characteristic features and indication of the tephra sampling location. Surveyed length: 594 m. Surveyed depth: 65 m. Surveyed by: Glacier Cave Explorers, Oregon High Desert Grotto, National Speleological Society, June 23–24, 2021. Surveyors: Sarah Burgess, Eduardo Cartaya, Scott Linn, Lee Florea, Christian Stenner. Cartography: Christian Stenner (UISv2 5–4-BCEF)
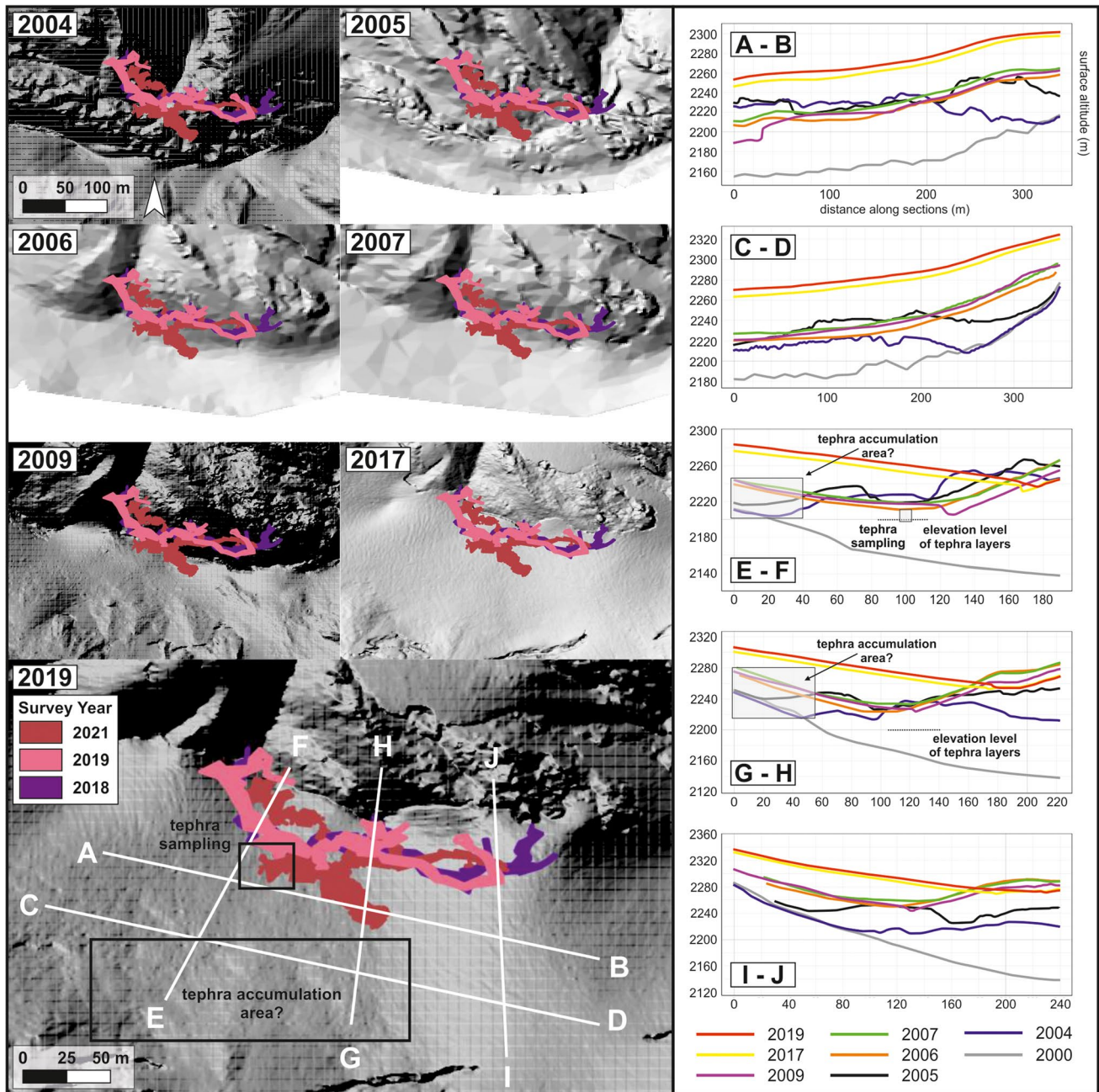
Fig. 8 Uppermost part of Crater Glacier and location of Mothra Cave. Shown here: Movement of the glacier-lava dome interface from 2004 to 2019 and extent and morphology changes of Mothra Cave from 2018 to 2021 (left). Elevation profiles indicate the development of the glacier from 2000 to 2019 (right). LiDAR data derive from the Washington LiDAR Portal, Messerich et al. (2008), and Mosbrucker (2020). The tephra sampling site and the potential accumulation area are indicated (black boxes)

areas persisted for years and can be assumed to be permanent (Fig. 5), although a quantification of heat fluxes only through visual observations was not possible. (3) In addition to the examples presented in Fig. 5, several further areas indicating heat release were identified using Google Earth. Based on these observations alone, we cannot identify which parts of the lava dome feature the highest thermal energy release, but we are able to characterize the spatial distribution of

heat release from the dome complex and its persistency over time. Although such visual observations represent a rather simple tool and do not result in quantifiable data, they can be helpful to better understand the lava dome complex and its interactions with the glacier. For example, by combining the visual observation of the glacier and lava dome, we are able to say which thermal features can be considered as permanent and which ones have changed over time, and which
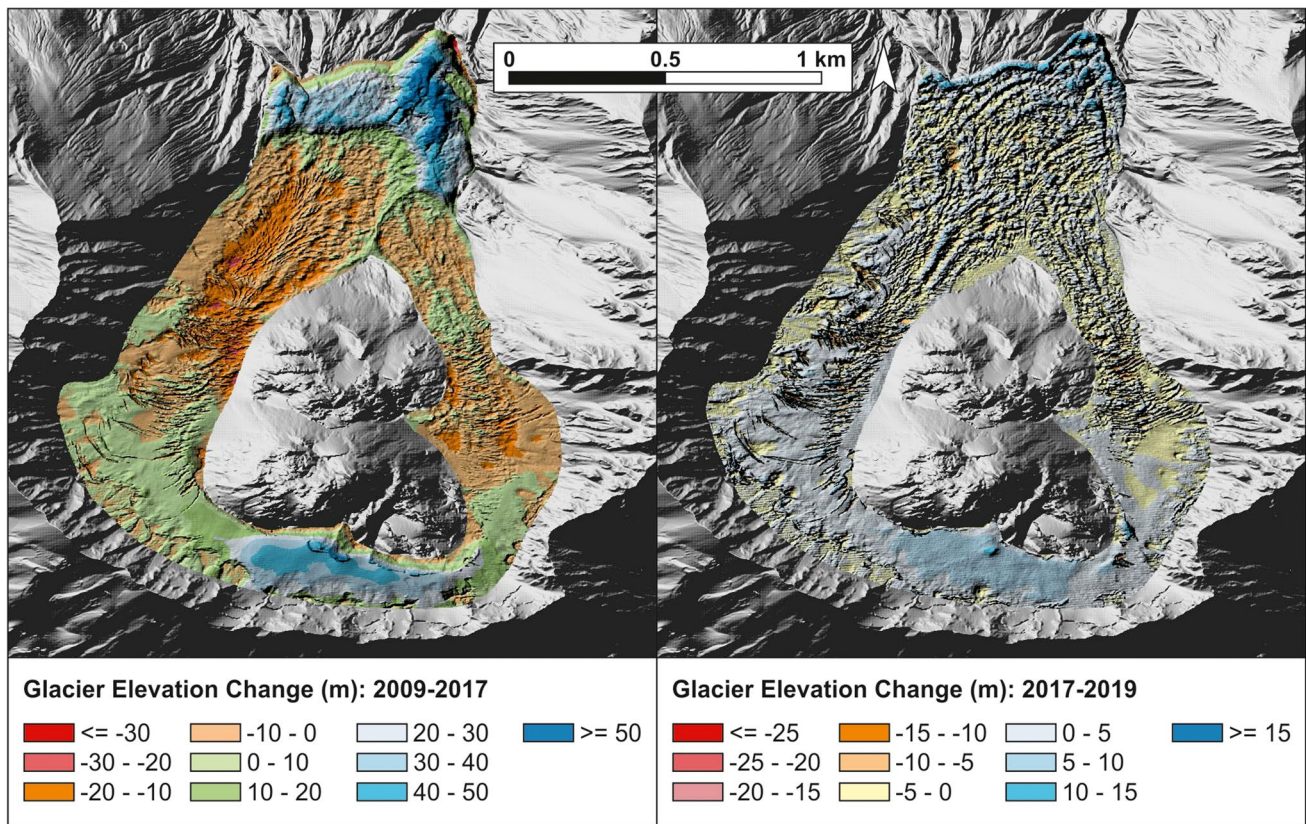
Fig. 9 Glacier elevation changes from 2009 to 2017 (left) and from 2017 to 2019 (right) based on LiDAR data provided by the Washington Lidar Portal

areas may form void spaces in the future in the case glacier encroachment continues into these areas.

Origin and deposition of subglacial tephra layers

Lava dome growth between 2004 and 2008 was characterized by several brief explosive events and minor venting of steam and ash with most prominent explosions occurring in October 2004, January 2005, and March 2005 (Scott et al. 2008). As we identified numerous layers of black and brownish volcanic material embedded in the glacier from within (Fig. 10), we aimed to characterize this material and determine its origin. Our results clearly suggest that at least two of four layers from the cave wall inside Mothra Cave (layers A and C) contain a juvenile component as discussed by Rowe et al. (2008a; 2008b), who investigated eruption material from 2004 to 2005. There, we identified type 1b glassy particles, which compositionally and texturally closely match 2004–2005 juvenile dome material. "Juvenile" as defined by Rowe et al. (2008a) comprises clean glass characterized by distinctly low MgO contents (<0.5 wt%) and comparatively high K_2O contents (between 3.5 and 5.5 wt%) at comparable SiO_2 contents. Type 1b particles have textural characteristics overlapping with material erupted from the

dome in 2004 (Cashman et al. 2008), and we thus interpret those to represent material form explosive events in 2004. Our type 1c groundmass glasses, found in layers C and D, have closely similar compositions to type 1b with similarly low MgO and high K_2O contents, except for somewhat lower SiO_2 contents of 67–70 wt%. Although such lower SiO_2 content glasses were not identified by Rowe et al. (2008a), we tentatively suggest that type 1c particles represent somewhat less evolved juvenile 2004–2008 dome material. Moderate crystallization of the phenocryst phases (orthopyroxene, plagioclase, Fe-Ti oxides, and quartz) may thus have provided a genetic link between the type 1c and 1b glass compositions. In conclusion, we positively identified juvenile 2004 dome material in layers A and C within Mothra Cave, which effectively represents the maximum deposition age of these layers. Also, the somewhat less evolved but compositionally very similar type 1c particles found in layers C and D may represent dome material from the 2004–2008 eruption cycle (Fig. 10).

The tephra layers sampled within Mothra Cave are clearly polygenetic, as a majority of the volcaniclastic particles do not originate from the 2004–2008 dome. The two main groups of non-juvenile material are dacites and rhyolites of variable compositions (type 1a) and variably mafic to
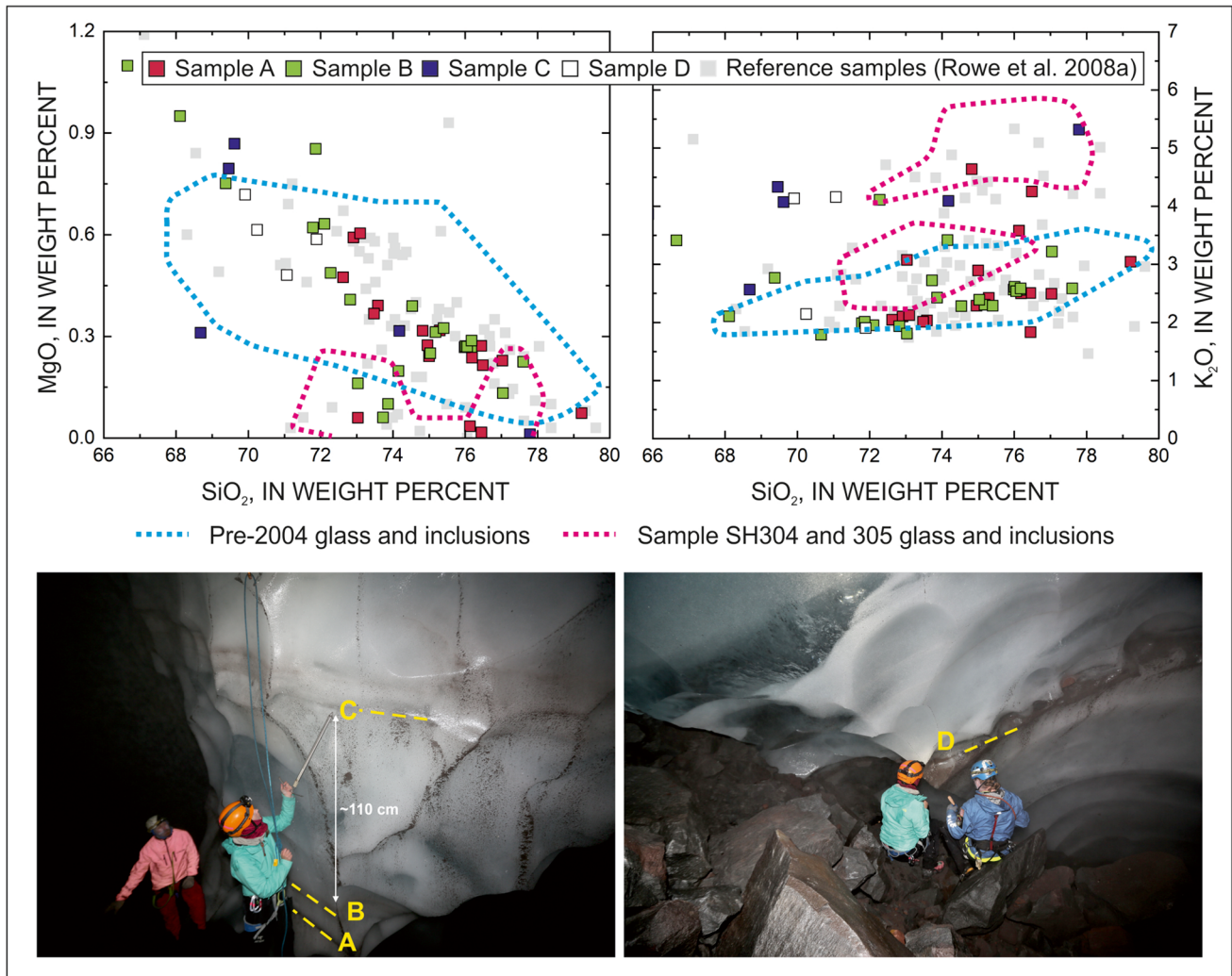
Fig. 10 Chemical variation diagrams of MgO and K$_2$O versus SiO$_2$ contents in clean groundmass glass. Colored square symbols in the plots illustrate the different tephra layers sampled in 2021. Reference fields comprise glass and melt inclusion compositions for dome samples SH304 and SH305 from 2004/2005 explosions (dashed magenta line), as well as pre-2004 tephra and dome glass compositions (dashed blue line) (cf. Rowe et al. 2008a). Although many analyzed grains from samples A and B have compositions similar to pre-2004 tephra, a subset of grains in samples A and B (and one grain in sample C) has the distinctly lower MgO and higher K$_2$O groundmass glass compositions that are similar to the juvenile components of the 2004–2005 dome samples and are most likely derived from that eruptive episode (within dashed magenta lines; Rowe et al. 2008a). See main text for discussion. Reference samples from Rowe et al. (2008a) are shown by gray symbols. Pre-2004 tephra and dome glass compositions derive from Sarna-Wojcicki et al. (1981) and Melson (1983); compositions for dome samples SH304 and SH305 from Pallister et al. (2008). Note: Three type 1a groundmass glasses have < 66 wt% SiO$_2$ and are not shown in the plots. Photos below show the tephra sampling inside Mothra Cave. Photo: Andreas Pflitsch

intermediate glassy particles (type 2). All four layers (A to D) contain the variably composed type 1a rhyolite to dacite particles, while two (A and B) additionally contain the more mafic type 2 particles. The obvious origin of these materials is as volcanic debris derived from the surrounding crater walls, representing various earlier eruption phases.

Several possibilities could explain the formation of the distinct subglacial tephra layers, including re-deposition and combinations of eolian and water transport mechanisms. Most particles have angular shapes, compatible with short transport distances from the nearby crater walls. Discrete

layers are volumetrically dominated by particles other than the juvenile ones from the 2004–2008 dome. The simplest explanation for layer formation would be comparatively rapid re-deposition of pre-mixed volcanic material from crater walls and dome explosions. Such re-deposition events may have been linked to enhanced earthquake activity during dome growth. Layers A and C show different grain sizes but a good sorting and homogeneous distribution within each individual layer, which could be a result of syn- or post-depositional sorting by strong winds. Sample D does not represent a homogeneous layer and seems to be the result of
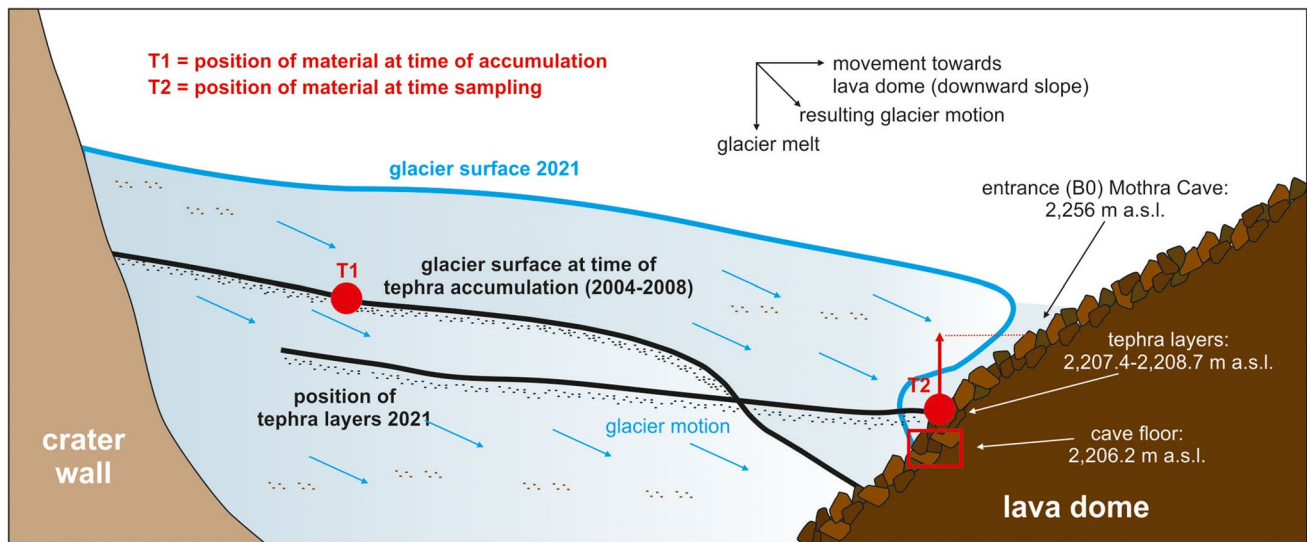
Fig. 11 A schematic cartoon of glacier surface changes and position changes of tephra layers embedded in the glacier. Not to scale

melt-freeze cycles with confluence and mixing of material. Our preferred model for the discrete layers is re-deposition temporally connected to the explosive dome activity periods. Based on our results, we are not able to say if the observed tephra layers can be linked to some of the major explosive events between October 2004 and March 2005 or to minor events occurring between 2004 and 2008.

Surface subsidence and glacier melt

By assuming an accumulation of tephra layers between 2004 and 2008 and by incorporating information from LiDAR data (Fig. 8), cave survey results (Fig. 7), and glacier movement (Fig. 2), we can speculate about glacier surface subsidence and melting. Given the uncertainties about the exact accumulation times and the precise location of material at the time of accumulation, estimations inherently have significant uncertainties. By determining the exact location of subglacial tephra samples in 2021 and identifying a juvenile component, however, we obtain the following information: (1) After more than 12 years since the end of the last eruption cycle, the glacier did not fully recharge its glacial masses in its uppermost part south of the new lava dome. Considering that we are still able to find material from 2004/2008 in this part of the glacier once more underlines the limited movement of ice toward the glacier arms in this area. Sufficient snow supply is the major factor for glacier mass increase, but melting processes and glacier flow also play a key role in this specific area. Glacier movement is comparatively small, and melting rates are definitely smaller than accumulation rates. (2) We can narrow down the net surface subsidence of the glacier to a maximum of ~ 40 m by assuming an accumulation between 2004 and 2005 and

to 50–80 m by including the time span from 2004 to 2008 (Fig. 11). Subsidence here is considered as the elevation difference between the possible tephra accumulation area and the sampling location in 2021.

Although this method has significant uncertainties, it is a novel idea of how to calculate glacier subsidence and melt and to take advantage of the unique characteristics of the Mount St. Helens crater. Due to the formation of glaciovolcanic caves around the new lava dome which provide access to the interior of the glacier, the tephra layers embedded in the ice are useful to further characterize volcano-ice interactions at Mount St. Helens and to obtain additional information about how the crater and glacier have changed after the last eruption cycle.

Future development of Crater Glacier

As suggested by Walder et al. (2010), Crater Glacier continued to grow after being perturbed by lava-dome emplacement between October 2004 and January 2008, advancing further down the Loowit channel and developing a steeply sloping toe. Substantial advance was also observed toward Step channel. Against expectations by Walder et al. (2010), we find that the glacier toe has become largely free of a rock-debris cover. LiDAR data showed that the glacier gained in volume (Fig. 9), and we expect this trend to continue in the next few years. However, we do not expect the rock content to decrease soon, as constant and significant rockfall still occurs. Based on our observations of the of glacier toe advance (Fig. 3a) and the development of the rock-ice interface at the new lava dome (Fig. 3b), we agree with Diefenbach (2017) who found glacier growth rates to be decreasing. Crater Glacier

features typical characteristics of a debris-covered glacier with numerous supraglacial ponds existing on the glacier surface. We expect the number of ponds to increase and existing ones to expand. The thick debris cover on the one hand and sufficient snow supply on the other hand secure glacier growth or at least a steady state which the glacier will likely reach in the next decades. We have to consider, however, that increasing temperatures and heat waves can have significant impact on the glacier as experienced in summer 2021. Considering the number of heat waves that hit the Pacific Northwest during the last two decades, e.g., 2006, 2009, and 2021 (Bumbaco et al. 2013; Overland 2021), and the assumption that heat waves will increase in both duration and intensity due to the current global warming (Clark et al. 2006), the accumulation area with its thin and patchy debris cover will be strongly affected by melting. Although there is enough snow supply and the crater provides sufficient shade at this point, this can drastically change if average temperatures rise in the near future.

We suggest the following phases of evolution for the Crater Glacier: (1) Rapid cooling of the dome surface from above, complemented by assumed increase of dome cooling from groundwater circulation through cracks. During this phase, heat flow and surface temperatures decreased rapidly, allowing for increased glacier growth rates. (2) Slowly diminishing overall heat flow from the dome leads to the attainment of a dynamic near-steady-state thermal balance at the dome-glacier interface, resulting in steady ice accumulation rates. (3) Increasing melting rates due to the increased effect of global warming; this is the presently evolving, and also a future, scenario.

Conclusions

After the end of the 2004–2008 eruption cycle, Crater Glacier continued to grow and adopted the features of a debris-covered glacier. Glacier advance in the uppermost part leads to the interaction of the glacier with the new lava dome. Due to this, glaciovolcanic caves formed, indicating areas of increased thermal energy release and the opposing situation of overall glacial accumulation combined with localized subglacial ablation.

The uppermost part of the glacier south of the new lava dome is still subject to significant snow accumulation caused by the limited transport of snow toward the sides. This was clearly indicated by an orthophoto generated from images taken in summer 2021. Instead of motion toward the sides, the glacier substantially gained in elevation with expansion toward the new lava dome. The location of the rock-ice interface, however, seems to have reached a temporary steady state as further advance is strongly affected by thermal energy release. The chemical compositions of tephra particles recovered from

discrete layers within Mothra cave revealed the existence of juvenile material likely related to the 2004–2008 eruption cycle. This allowed a rough calculation of glacier surface subsidence and movement since that time and provided partial insight into subglacial processes.

Mount St. Helens offers a unique opportunity to investigate a glacier growing in times of global warming and glacier shrinkage and represents an outstanding environment to observe both the evolution and transformation of a glacier defying climate change and a glacier strongly interacting with an active volcano. Our investigations show how Crater Glacier has changed since the end of the last eruption cycle and which methods can be used to obtain information about glacial processes and interactions with the volcanic edifice. This extends our understanding of volcano-ice interactions and may be applicable to other glacier-covered volcanoes worldwide.

References

Anderson LS, Anderson RS (2018) Debris thickness patterns on debris-covered glaciers. Geomorphology 311:1–12. https://doi.org/10.1016/j.geomorph.2018.03.014

Anderson CH, Vining MR (1999) Observations of glacial, geomorphic, biologic, and mineralogic developments in the crater of Mount St. Helens, Washington. Wash Geol 27:9–19

Anderson CH, Behrens CJ, Floyd GA, Vining MR (1998) Crater firn caves of Mount St. Helens. Wash JCKS 60:44–50

Bailey JE, Dehn J (2006) Volcano monitoring using Google Earth. In: Brady SR, Sinha AK, Gundersen LC (eds.) Geoinformatics 2006—abstracts: U.S. Geological Survey Scientific Investigations Report 2006–5201, 60

Bergfeld D, Evans WC, McGee KA, Spicer KR (2008) Pre- and post-eruptive investigations of gas and water samples from Mount St. Helens, Washington, 2002 to 2005. In: Sherrod DR, Scott WE, Stauffer PH (eds) A volcano rekindled: the renewed eruption of Mount St. Helens, 2004–2006: U.S. Geological Survey Professional Paper 1750 523–542

Bumbaco KA, Dello KD, Bond NA (2013) History of Pacific Northwest heat waves: synoptic pattern and trends. J Appl Meteorol Climatol 52:1618–1631. https://doi.org/10.1175/JAMC-D-12-094.1

Cashman KV, Thornber CR, Pallister JS (2008) From dome to dust: shallow crystallization and fragmentation of conduit magma during the 2004–2006 dome extrusion of Mount St. Helens, Washington, in Sherrod DR, Scott WE, Stauffer PH (eds) A volcano rekindled: the renewed eruption of Mount St. Helens, 2004–2006: U.S. Geological Survey Professional Paper 1750 387–413.

Clark RT, Brown SJ, Murphy JM (2006) Modeling Northern Hemisphere summer heat extreme changes and their uncertainties using a physics ensemble of climate sensitivity experiments. J Clim 19:4418–4435. https://doi.org/10.1175/JCLI3877.1

Department of Natural Resources (2022) Washington LiDAR Portal. https://lidarportal.dnr.wa.gov/#44.37099:-155.43457:4

Diefenbach A (2017) Monitoring changes to Crater Glacier at Mount St. Helens. https://eros.usgs.gov/doi-remote-sensing-activities/2017/usgs/monitoring-changes-crater-glacier-mount-st-helens. Accessed 4 Jan 2023

Gabrielli S, Spagnolo M, de Siena L (2020) Geomorphology and surface geology of Mount St Helens volcano. J Maps 16:585–594. https://doi.org/10.1080/17445647.2020.1790048

Gutro R, Puckett C (2004) Laser technology helps track changes in Mount St. Helens. NASA's Goddard Space Flight Center. https://www.nasa.gov/vision/earth/lookingatearth/mshelenslidar.html. Accessed 4 Jan 2023

Hunt JB, Hill PG (2001) Tephrological implications of beam size—sample-size effects in electron microprobe analysis of glass shards. J Quaternary Sci 16:105–117. https://doi.org/10.1002/jqs.571

James MR, Antoniazza G, Robson S, Lane SN (2020b) Mitigating systematic error in topographic models for geomorphic change detection: accuracy, precision and considerations beyond off-nadir imagery. Earth Surf Process Landforms 45:2251–2271. https://doi.org/10.1002/esp.4878

James M, Carr B, D'Arcy F, Diefenbach A, Dieterich H, Fornaciai A, Lev E, Liu E, Pieri D, Rodgers M, Smets B, Terada A, Aulock F von, Walter T, Wood K, Zorn E (2020a) Volcanological applications of unoccupied aircraft systems (UAS): developments, strategies, and future challenges. Volcanica:67–114 https://doi.org/10.30909/vol.03.01.67114

Jarosewich E, Nelen JA, Norberg JA (1980) Reference samples for electron microprobe analysis. Geostand Geoanal Res 4:43–47. https://doi.org/10.1111/j.1751-908X.1980.tb00273.x

Liu M, Chen N, Zhang Y, Deng M (2020) Glacial lake inventory and lake outburst flood/debris flow hazard assessment after the Gorkha Earthquake in the Bhote Koshi Basin. Water 12:464. https://doi.org/10.3390/w12020464

Lundstrom SC, McCafferty AE, Coe JA (1993) Photogrammetric analysis of 1984–89 surface altitude change of the partially debris-covered Eliot Glacier, Mount Hood, Oregon, U.S.A. Ann Glaciol 17:167–170

Martin MD, Barr I, Edwards B, Spagnolo M, Vajedian S, Symeonakis E (2021) Assessing the use of optical satellite images to detect volcanic impacts on glacier surface morphology. Remote Sensing 13:3453. https://doi.org/10.3390/rs13173453

Melson WG (1983) Monitoring the 1980–1982 eruptions of Mount St. Helens: compositions and abundances of glass. Science 221:1387–1391. https://doi.org/10.1126/science.221.4618.1387

Messerich JA, Schilling SP, Thompson RA (2008) Digital elevation models of the pre-eruption 2000 crater and 2004–07 dome-building eruption at Mount St. Helens, Washington, USA: U.S. Geological Survey Open-File Report 2008–1169, 2 p. https://pubs.usgs.gov/of/2008/1169/

Mihalcea C, Mayer C, Diolaiuti G, D'Agata C, Smiraglia C, Lambrecht A, Vuillermoz E, Tartari G (2008) Spatial distribution of debris thickness and melting from remote-sensing and meteorological data, at debris-covered Baltoro glacier, Karakoram. Pakistan Ann Glaciol 48:49–57. https://doi.org/10.3189/172756408784700680

Miles KE, Hubbard B, Irvine-Fynn TD, Miles ES, Quincey DJ, Rowan AV (2020) Hydrology of debris-covered glaciers in High Mountain Asia. Earth-Sci Rev 207:103212. https://doi.org/10.1016/j.earscirev.2020.103212

Mills HH (1992) Post-eruption erosion and deposition in the 1980 crater of Mount St Helens, Washington, determined from digital maps. Earth Surf Process Landforms 17:739–754. https://doi.org/10.1002/esp.3290170803

Mosbrucker AR (2014) High-resolution digital elevation model of Mount St. Helens crater and upper North Fork Toutle River basin, Washington, based on an airborne lidar survey of September 2009: U.S. Geol Surv Data Ser 904. https://doi.org/10.3133/ds904

Mosbrucker AR (2020) High-resolution digital elevation model of Mount St. Helens and upper North Fork Toutle River basin, based on airborne lidar surveys of July-September, 2017: U.S. Geol Surv data release. https://doi.org/10.5066/P9H16RC7

Nicholson L, Benn DI (2006) Calculating ice melt beneath a debris layer using meteorological data. J Glaciol 52:463–470. https://doi.org/10.3189/172756506781828584

Østrem G (1959) Ice melting under a thin layer of moraine, and the existence of ice cores in moraine ridges. Geogr Ann 41:228–230. https://doi.org/10.1080/20014422.1959.11907953

Overland JE (2021) Causes of the record-breaking Pacific Northwest Heatwave, Late June 2021. Atmosphere 12:1434. https://doi.org/10.3390/atmos12111434

Pallister JS, Thornber CR, Cashman KV, Clynne MA, Lowers HA, Mandeville CW, Brownfield IK, Meeker GP (2008) Petrology of the 2004–2006 Mount St. Helens lava dome—implications for magmatic plumbing and eruption triggering, in Sherrod DR, Scott WE, Stauffer PH (eds) A volcano rekindled: the renewed eruption of Mount St. Helens, 2004–2006: U.S. Geol Surv Prof Paper 1750 647–702

Price SF, Walder JS (2007) Modeling the dynamic response of a crater glacier to lava-dome emplacement: Mount St Helens, Washington. USA Ann Glaciol 45:21–28. https://doi.org/10.3189/172756407782282525

Rowe MC, Kent A, Thornber CR (2008b) Using amphibole phenocrysts to track vapor transfer during magma crystallization and transport: an example from Mount St. Helens, Washington. J Volcanol Geoth Res 178:593–607. https://doi.org/10.1016/j.jvolgeores.2008.01.012

Rowe MC, Thornber CR, Kent AJR (2008a) Identification and evolution of the juvenile component in 2004–2005 Mount St. Helens ash, in Sherrod DR, Scott WE, Stauffer PH (eds) A volcano rekindled: the renewed eruption of Mount St. Helens, 2004–2006: U.S. Geol Surv Prof Paper 1750 629–646

Sarna-Wojcicki AM, Meyer CE, Woodward MJ, Lamothe PJ (1981) Composition of air-fall ash erupted on May 18, May 25, June 12, July 22, and August 7, *in* Lipman PM, Mullineaux DR (eds) The 1980 eruptions of Mount St. Helens, Washington: U.S. Geological Survey Professional Paper 1250 667–681.

Schilling SP, Carrara PE, Thompson RA, Iwatsubo EY (2004) Postereuption glacier development within the crater of Mount St. Helens, Washington. USA Quat Res 61:325–329. https://doi.org/10.1016/j.yqres.2003.11.002

Scott WE, Sherrod DR, Gardner CA (2008) Overview of the 2004 to 2006, and continuing, eruption of Mount St. Helens, Washington, *in* Sherrod DR, Scott WE, Stauffer PH (eds) A volcano rekindled: the renewed eruption of Mount St. Helens, 2004–2006: U.S. Geological Survey Professional Paper 1750 3–23.

Sobolewski L, Stenner C, Hueser C, Berghaus T, Cartaya E, Pflitsch A (2022) Ongoing genesis of a novel glaciovolcanic cave system in the crater of Mount St. Helens, Washington, USA. JCKS 84:51–65. https://doi.org/10.4311/2021ES0113

Stenner C, Pflitsch A, Florea L, Graham K, Cartaya E (2022) Development and persistence of hazardous atmospheres in a glaciovolcanic cave system—Mount Rainier, Washington, USA. JCKS 84:66–82. https://doi.org/10.4311/2021EX0102

Walder JS, LaHusen RG, Vallance JW, Schilling SP (2007) Emplacement of a silicic lava dome through a crater glacier: Mount St Helens, 2004–06. Ann Glaciol 45:14–20. https://doi.org/10.3189/172756407782282426

Walder SJ, Schilling SP, Vallance JW, LaHusen RG (2008) Effects of lava-dome growth on the Crater Glacier of Mount St. Helens, Washington, *in* Sherrod DR, Scott WE, Stauffer PH (eds) A volcano rekindled: the renewed eruption of Mount St. Helens, 2004–2006: U.S. Geological Survey Professional Paper 1750 257–273

Walder JS, Schilling SP, Sherrod DR, Vallance JW (2010) Photographic documentation of the evolution of Crater Glacier, Mount St. Helens, Washington, September 2006–November 2009: U.S. Geological Survey Open-File Report 2010–1141, 34 p. and animation. https://pubs.usgs.gov/of/2010/1141/

Westoby MJ, Brasington J, Glasser NF, Hambrey MJ, Reynolds JM (2012) 'Structure-from-motion' photogrammetry: a low-cost, effective tool for geoscience applications. Geomorphology 179:300–314. https://doi.org/10.1016/j.geomorph.2012.08.021